

1 **Improved catalytic activity of mixed platinum catalysts supported on various**
2 **carbon nanomaterials**

3 Jie Zhang^{a,b,c}, Shuihua Tang^{a,b,*}, Longyu Liao^c, Weifei Yu^{c,*}, Jinshan Li^c, Frode
4 Seland^d, Geir Martin Haarberg^d

5 ^a*State Key Laboratory of Oil and Gas Reservoir Geology and Exploitation, Southwest*
6 *Petroleum University, Chengdu City, Sichuan 610500, PR China*

7 ^b*School of Materials and Engineering, Southwest Petroleum University, Chengdu*
8 *City, Sichuan 610500, PR China*

9 ^c*Institute of Chemical Materials, China Academy of Engineering Physics, Mianyang*
10 *City, Sichuan 621900, PR China*

11 ^d*Department of Materials Science and Engineering, Norwegian University of Science*
12 *and Technology, Trondheim 7491, Norway*

13 *Corresponding author. Tel | Fax: +86 028 83032879.

14 E-mail address: shuihuatang@swpu.edu.cn (S.H. Tang).

15 Corresponding author. Tel | Fax: +86 0816 2480362.

16 E-mail address: yuwf_1988@sohu.com (W.F. Yu).

17

18 **ABSTRACT**

19 Electrocatalyst support affects not only catalytic activity of a catalyst, but also mass
20 transportation and electron transfer in the catalyst layer of an electrode for proton
21 exchange membrane fuel cells. Multi-dimensional and combined carbon materials
22 such as Vulcan XC-72, carbon nanotubes (CNTs), and home-made coiled carbon
23 nanotubes (CCNTs) are applied to enhance the catalyst activity and utilization. Three-
24 dimensional CCNTs with large specific surface area and good graphitic characteristic
25 are synthesized by solid-state catalytic method. This obtained CCNTs and commercial
26 CNTs are used as support to prepare platinum catalysts via a modified ethylene glycol
27 method, respectively. The electrochemical surface areas (ECSAs) of the as-prepared
28 Pt/CNTs, Pt/CCNTs, and commercial Pt/C (JM) catalyst are evaluated by cyclic
29 voltammetry. Then each two and three kinds of above catalysts mixed with different
30 mass ratios are investigated. The ECSAs of Pt/C-Pt/CCNTs (95:5) and Pt/C-Pt/CNTs-
31 Pt/CCNTs (80:10:10) are calculated to be $106 \text{ m}^2 \text{ g}_{\text{Pt}}^{-1}$ and $111 \text{ m}^2 \text{ g}_{\text{Pt}}^{-1}$, with respect to
32 $70 \text{ m}^2 \text{ g}_{\text{Pt}}^{-1}$ of Pt/C (JM) catalyst. And these mixed catalysts also demonstrate
33 improved oxygen reduction reaction activities. This is mainly attributed to the unique
34 structure of CCNTs, which can construct a multi-dimensional network to facilitate the
35 mass transportation and electrons/protons transfer.

36 *Keywords:*
37 Coiled carbon nanotubes
38 Carbon nanotubes
39 Oxygen reduction reaction
40 Catalytic activity
41 Proton exchange membrane fuel cells

42

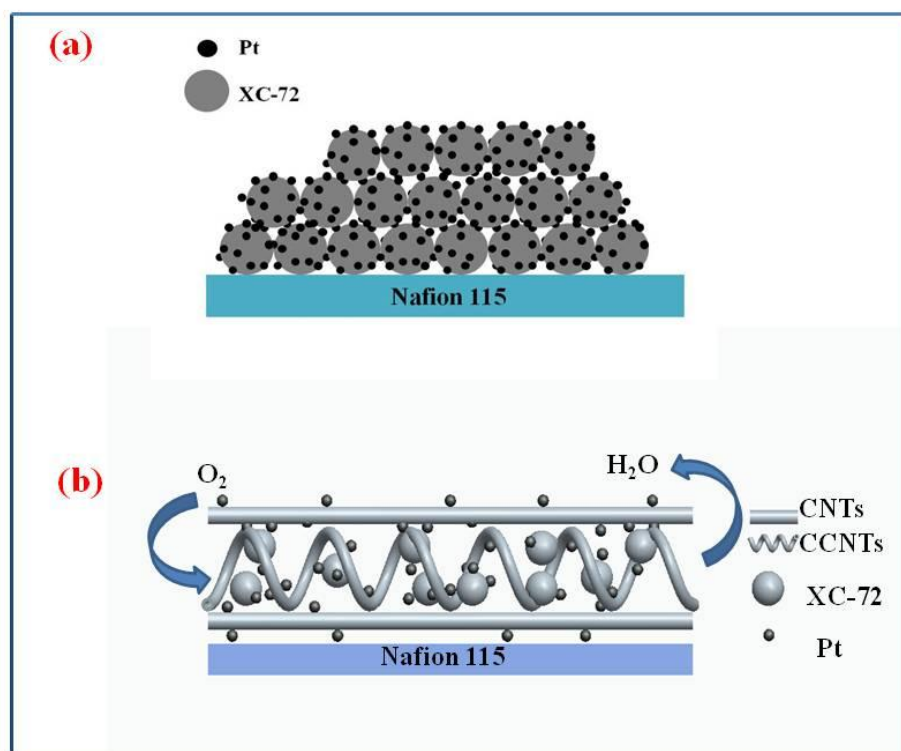
43 **1. Introduction**

44 Proton exchange membrane fuel cell (PEMFC) has been regarded as an attractive and
45 efficient power supply for portable applications due to its high efficiency, high
46 specific energy density, zero pollution, and low operating temperature [1-2]. Pt-based
47 electrocatalysts, a kind of promising catalytic materials for widely-adapted PEMFC,
48 provide remarkable activity for hydrogen oxidation and oxygen reduction reactions
49 (ORR) [3]. One important goal for commercialization of PEMFC is to reduce the
50 amount of platinum and enhance the cell performance [4]. It is generally accepted that
51 the performance depends on the shape, size, and distribution of Pt nanoparticles. In
52 addition, supporting material could affect not only the catalytic properties but also
53 mass transport and electron transfer in catalyst layers of the electrode, resulting in an
54 enhanced catalytic activity [5]. Various carbon materials with different nanostructures
55 and morphological characteristics have been used as support ranging from carbon
56 black, carbon aerogels, carbon nanotubes, and mesoporous carbon. Carbon black
57 Vulcan XC-72 has been commonly used as support for electrocatalysts in PEMFC,
58 but the utilization of XC-72 supported catalyst is usually less than 20% due to a close
59 packing of catalyst particles during the hot-pressing process of membrane electrode
60 assembly (MEA) fabrication [7]. Carbon nanotubes (CNTs), with the unique
61 morphology and physical properties including a large aspect ratio, good electrical
62 conductivity, and mechanical stability, possess the ability to carry large current
63 densities and offer channels for fast electron/proton transfer when used for PEMFC
64 [8-10]. The carbon nanocoils (CNCs) also realize the requirement of an ideal support
65 for electrocatalysts, mainly due to well-defined porosity, large specific surface area of
66 $318 \text{ m}^2 \text{ g}^{-1}$, high degree of graphitization, and good crystallinity [11].

67 Recently the potential application of mixed electrocatalysts has been proposed to
68 enhance the electrochemical properties. Single-wall carbon nanotubes (SWNTs) and
69 multi-wall carbon nanotubes (MWNTs) hybrids loaded with Pt, evaluated as the
70 cathode catalyst layer in PEMFC, leading to an increased mass transport
71 characteristics and cathode-specific mass activity due to a combination of the
72 increased mass activity caused by MWNTs and the efficient proton transfer ensured
73 by the SWNT network [12]. Shaijumon et al. [13] used [50% Pt/MWCNT + 50%

74 Pt/C] as cathode electrocatalyst in PEMFC, and it showed the best performance of
 75 288.9 mW cm^{-2} at a voltage of 540 mV and a current density of 535 mA cm^{-2} due to
 76 better dispersion of Pt nanoparticles and good accessibility of MWCNT. Graphene
 77 nanosheet (GN) has also opened up a new way to be employed as support due to its
 78 unique morphology and high electronic conductivity [14-15]. Yang et al. [16]
 79 reported that the Pd/GNS-CNTs (GN/CNTs=5:1) exhibited the highest
 80 electrochemical active surface area (ECSA) and Pd utilization, which indicated the
 81 excellent catalytic activity and stability for formic acid electrooxidation compared to
 82 Pd/Vulcan XC-72R, Pd/GNS, or Pd/CNTs catalysts. Jafri et al. [17] pointed out that
 83 the mixture of functionalized multi-walled carbon nanotube (f-MWNT) and
 84 functionalized graphene (f-G) could also act as good catalyst supporting materials for
 85 both methanol oxidation and ORR. The single cell with PtRu/ (50% f-G + 50% f-
 86 MWNT) and Pt/ (50% f-G + 50% f-MWNT) gave a maximum power density of 68
 87 mW cm^{-2} .

88



89

90 **Fig. 1.** The schematic structures of catalyst layers. (a) Pt/XC-72 and (b) Pt/XC-72-
 91 Pt/CNTs-Pt/CCNTs

92 The structures of Pt/XC-72 and Pt/XC-72-Pt/CNTs-Pt/CCNTs catalyst layers are
 93 shown schematically in Fig. 1. Spherical XC-72 carbon black is a good catalyst
 94 support but its supported Pt catalysts are easily compressed during the hot-pressing
 95 process, as this will block reactants to get access to some active sites and reduce the
 96 catalyst utilization (as shown in Fig.1a). Moreover, the electron conductivity of XC-

97 72 is not very good. In this paper, three-dimensional coiled carbon nanotubes
98 (CCNTs) with large specific surface area and graphitic characteristic will be applied
99 to construct more effective mass transport channels, and one-dimensional CNTs are
100 expected to facilitate the electron transfer (as shown in Fig.1b). The introduction of
101 CCNTs and/or CNTs into the Pt/XC-72 catalysts will be designed to improve the
102 catalytic activity and utilization of Pt/XC-72. Both two and three types of Pt/C,
103 Pt/CNTs, and Pt/CCNTs catalysts will be mixed with different mass ratios and then
104 investigated.

105 **2. Experimental**

106 *2.1. Preparation of CCNTs*

107 CCNTs was synthesized according to the method of heat-treating mixtures of carbon
108 precursors, silica sol, and transition-metal salts [18]. Resorcinol-formaldehyde (RF)
109 gel was chosen as carbon precursor. Iron nitrate was used as catalyst, and silica sol
110 (AkzoNobel chemicals Corp., particle size of $\text{SiO}_2 = 4 \text{ nm}$; density = 1.1 g cm^{-3}) was
111 added to the reaction mixture to achieve a high specific surface area and suitable pore
112 size carbon material. The aqueous reaction mixture of iron nitrate/trisodium
113 citrate/silica/resorcinol/formaldehyde with a molar ratio of 0.8:0.8:1:2:4, was cured at
114 $85 \text{ }^\circ\text{C}$ for 3 h, then carbonized in an argon atmosphere at $850 \text{ }^\circ\text{C}$ for 3 h, followed by
115 refluxing in 3 M NaOH to remove the silica particles and in 5 M HNO_3 to remove
116 other residuals. Eventually CCNTs were obtained after filtering, washing, and drying
117 at $100 \text{ }^\circ\text{C}$ in vacuum overnight.

118 *2.2. Preparation of electrocatalysts*

119 Pt catalyst supported on carbon material was prepared by using an improved ethylene
120 glycol method. The required amount of chloroplatinic acid ($\text{H}_2\text{PtCl}_6 \cdot 6\text{H}_2\text{O}$) was added
121 to ethylene glycol (EG) under magnetic stirring, and then the pH value of the solution
122 was adjusted with sodium hydroxide. Subsequently, the required amounts of CNTs
123 (Chengdu Organic Chemicals Company, China) or CCNTs were added into the
124 resulting EG solution and the obtained reaction mixture was kept at $140 \text{ }^\circ\text{C}$ for 3 h
125 with an ongoing reduction process. Finally, the resulting suspension was cooled,
126 filtered, and washed with deionized water until no chloride ions were detected, and
127 then dried in a vacuum oven. The prepared catalysts are respectively denoted as 40
128 wt.% Pt/CNTs and 40 wt.% Pt/CCNTs. 40 wt.% Pt/C catalyst from Johnson Matthey
129 Company (HiS...) was adopted as Pt/XC-72.

130 *2.3. Physical characterization*

131 The Brunauer-Emmett-Teller (BET) specific surface areas were measured by N_2
132 adsorption and the Barrett-Joyner-Halenda (BJH) desorption method was applied to
133 determine pore size distributions, using on a Quantachrome Nova Automated Gas
134 Sorption System. The crystallinity of carbon materials and electrocatalysts was
135 determined through X-ray diffraction (XRD) performed on a Rigaku D/MAX X-ray

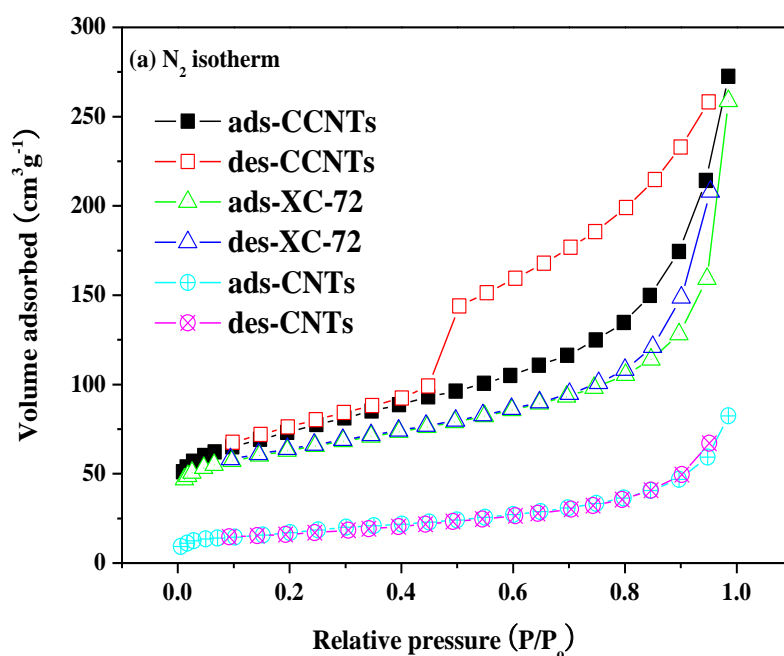
136 diffractometer equipped with Cu K α radiation operating at 40 kV and 40 mA. Raman
137 spectra were measured at room temperature with the Raman system (JY-HR800).
138 Morphologies of carbon material and catalysts were revealed by transmission electron
139 microscopy (TEM, Carl Zeiss SMT, Libra 200FE).

140 2.4. Electrochemical characterization

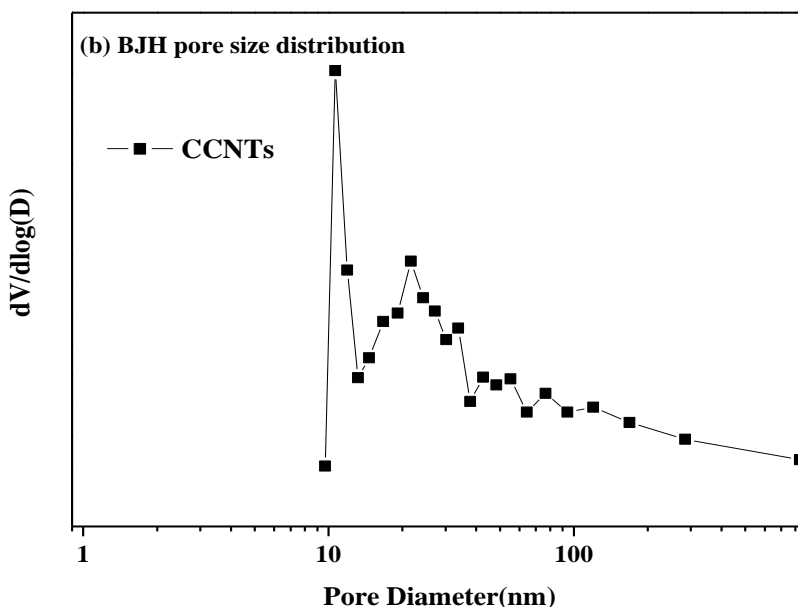
141 Electrochemical measurements were performed using an AutoLab Potentiostat
142 (Metrohm, Holland) with a three-electrode system at room temperature. 5 mg of the
143 electrocatalyst was ultrasonically suspended in 1 mL of ethanol and 50 μ L of Nafion[®]
144 solution (5 wt%, Du Pont) for 30 min to form a homogeneous ink. Then 25 μ L of the
145 ink was spread onto the surface of a glassy carbon electrode (GC) with a diameter of 5
146 mm (geometric area of 0.196 cm²) embedded in a Teflon cylinder (Pine Instrument).
147 A Pt wire and Ag/AgCl electrode were employed as the counter and the reference
148 electrodes, respectively. Cyclic voltammetry (CV) was performed at room
149 temperature between -0.2 and +1.2 V in 0.5 M H₂SO₄ with a scan rate of 20 mV s⁻¹.
150 Rotating disk electrode (RDE) experiments were conducted in O₂-saturated 0.5 M
151 H₂SO₄ from 1.0 to 0.45 V at a scan rate of 10 mV s⁻¹ and rotation rate of 1600 rpm.

152 3. Results and discussion

153 3.1. Physical characterization of carbon materials and electrocatalysts



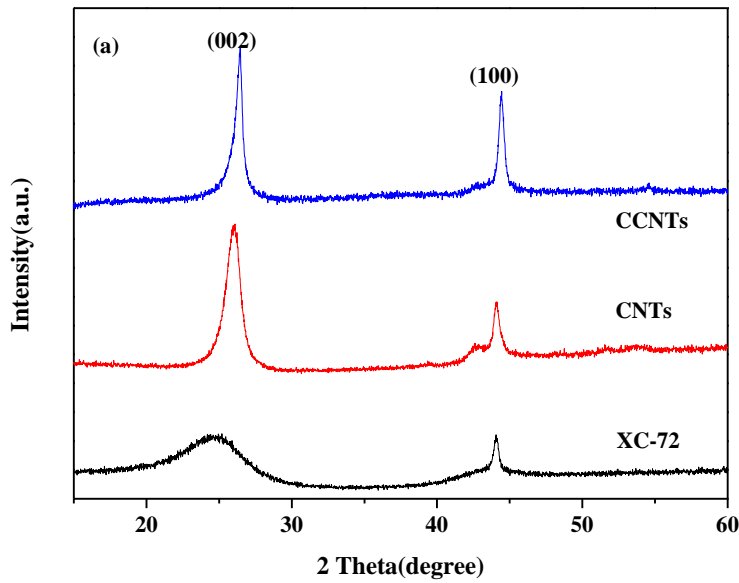
154



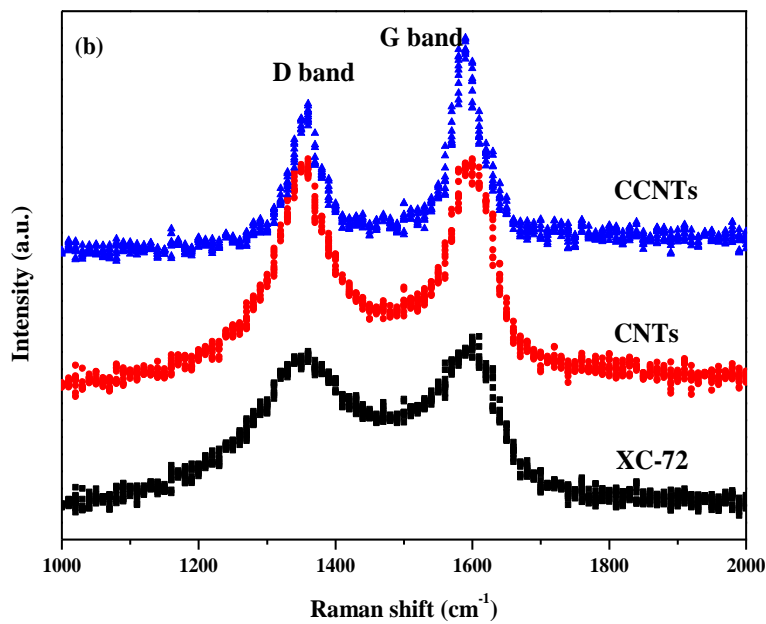
155

156 **Fig. 2.** (a) N_2 adsorption/desorption isotherm of carbon materials and (b) pore size
 157 distribution of CCNTs.

158 The specific surface areas of XC-72, CNTs, and CCNTs are measured to be 215, 61,
 159 and $404 \text{ m}^2 \text{ g}^{-1}$. The increased adsorption branch at low relative pressure and the
 160 hysteresis loop for desorption branch under the higher relative pressures of CCNTs
 161 are observed in Fig. 2a, which attributes to the hysteresis loop of type-H1 [19]. Fig.
 162 2b shows a pore distribution of CCNTs mainly ranging from 10 to 40 nm, which
 163 indicates a typical mesoporous structure. XC-72 possesses a significant amount of
 164 mesopores [20], but CCNTs exhibit much larger mesopore volume and specific
 165 surface area than those of XC-72 and CNTs.



166

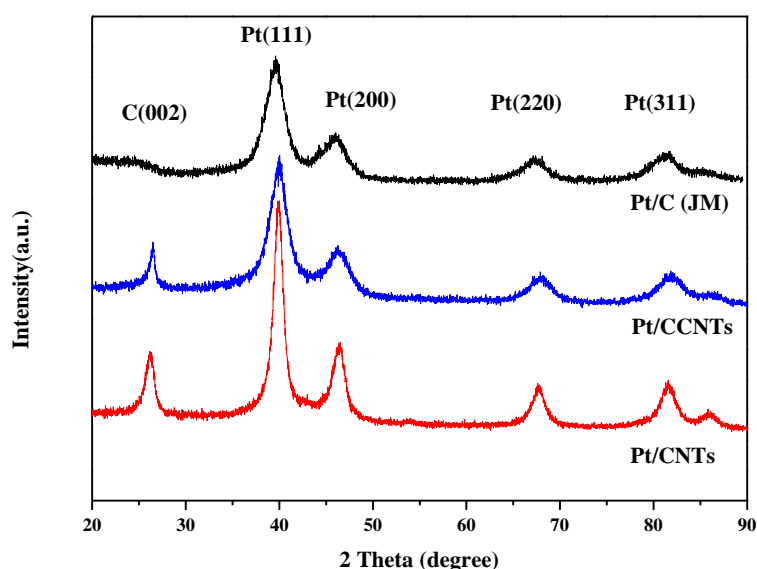


167

168 **Fig. 3.** (a) XRD patterns and (b) Raman spectra of various carbon materials.

169 Fig. 3a shows the XRD patterns of XC-72, CNTs, and CCNTs. It can be seen that
 170 CCNTs indicate intensive diffraction peaks corresponding to the (002) and (100)
 171 diffraction peaks of graphite. The (002) diffraction peak of CCNTs is sharper and
 172 more intense than that of the XC-72 or CNTs, indicating its excellent graphitic
 173 properties. Compared to 0.3354 nm of graphite $d_{(002)}$ spacing () [21], the $d_{(002)}$ of
 174 CCNTs is calculated to be 0.3387 nm using Bragg's equation based on the (002)

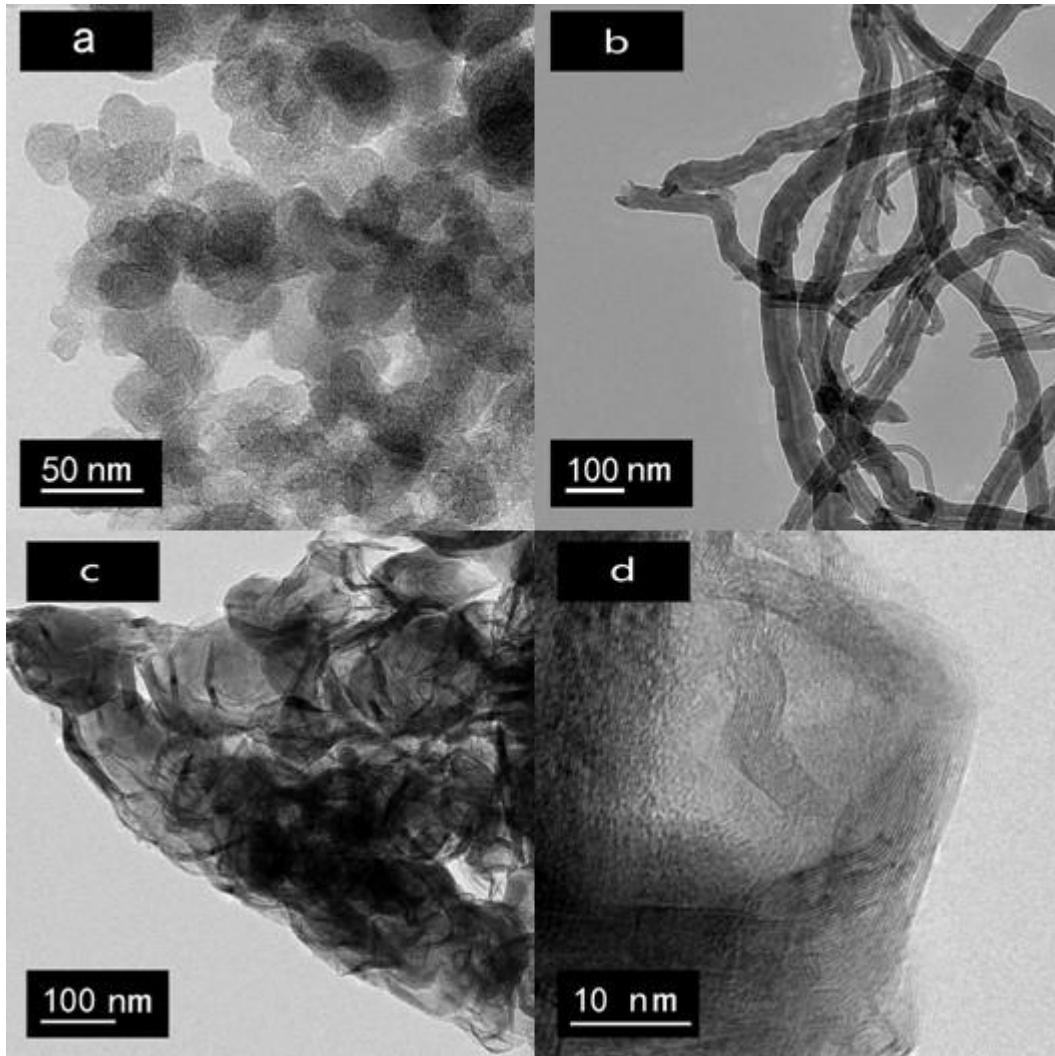
175 diffraction peak, and its crystallinity is superior to that of CNTs (0.3438 nm) or
 176 amorphous XC-72 (0.3678 nm) [22].. According to Raman spectra, a G (“graphite”)
 177 band peak at 1590 cm^{-1} relates to the vibration of sp^2 -hybridized carbon, a D
 178 (“defect”) band peak at 1350 cm^{-1} corresponds to defects, and the intensity ratio
 179 between the D and G bands (I_D/I_G) is a measure of graphitic characteristic, and the
 180 lower I_D/I_G value means a higher graphitic property [23]. As shown in Fig. 3b,
 181 CCNTs possess a lower I_D/I_G value than XC-72 and CNTs, which means it has better
 182 graphitic characteristic. This further confirms the XRD results.



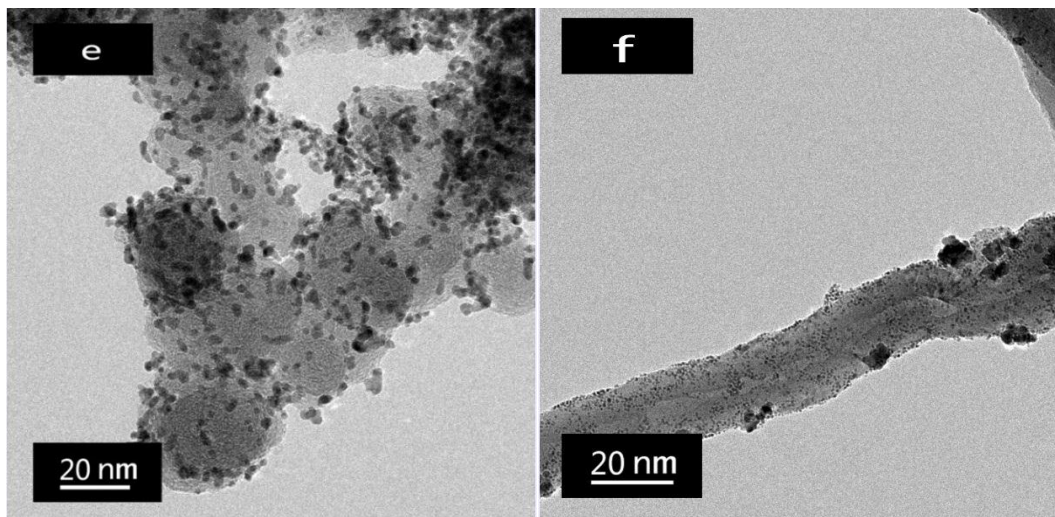
183

184 **Fig. 4.** XRD patterns of Pt catalysts supported on different carbon materials.

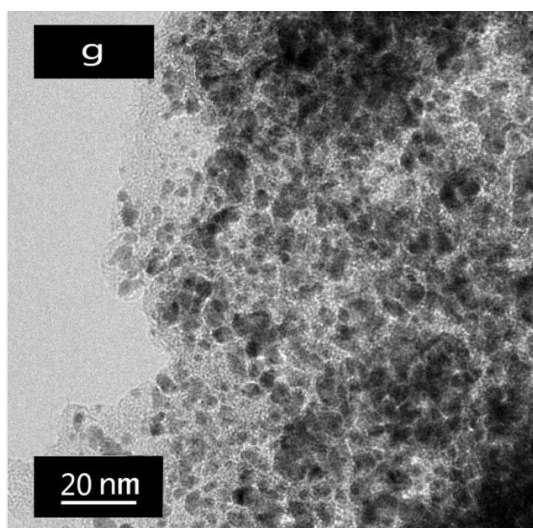
185 The XRD patterns in Fig. 4 show a f.c.c. Pt crystalline structure of Pt/CCNTs,
 186 Pt/CNTs, and Pt/C, which is inferred from Pt (111), (200), (220), and (311) four
 187 characteristic peaks located at 39.8° , 46.2° , 67.5° , and 81.2° . The Pt (220) peak is
 188 isolated from the graphite diffraction peaks of carbon support [24], and the mean size
 189 of the Pt particles in Pt/CCNTs, Pt/CNTs, and Pt/C are calculated to be 3.7 nm, 5.8
 190 nm, and 3.5 nm via Scherrer’s formula.



191



192

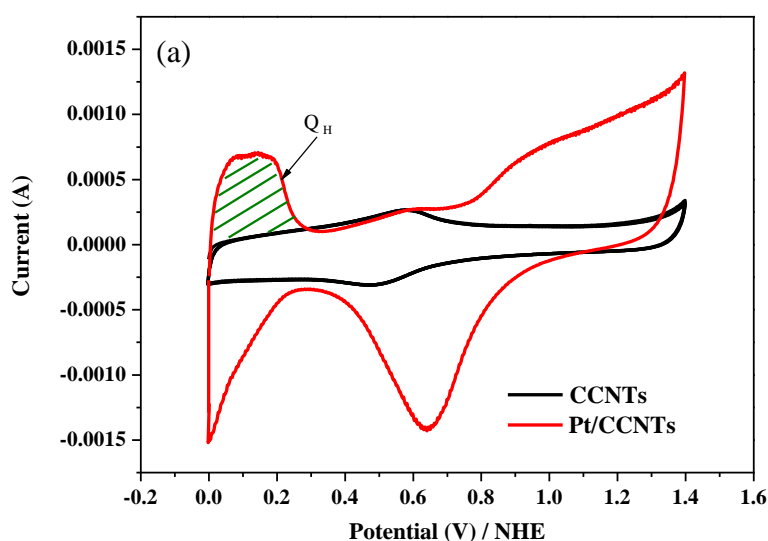


193

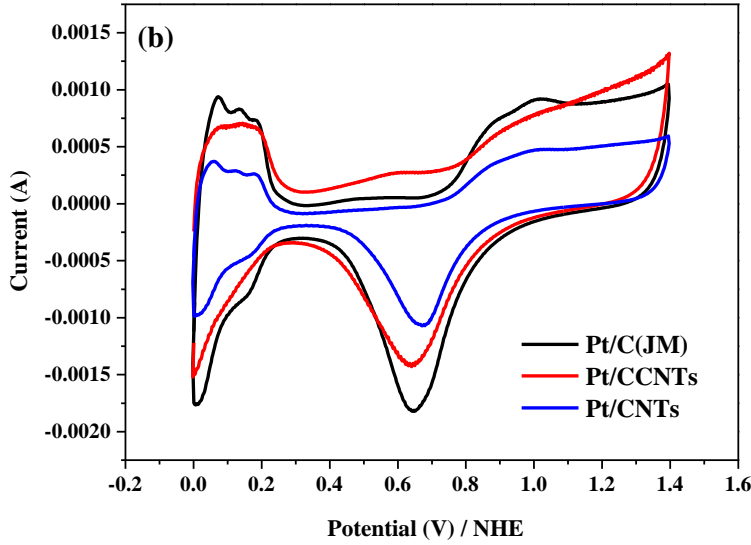
194 **Fig. 5.** TEM images of (a) XC-72, (b) CNTs, (c) and (d) CCNTs, (e) Pt/C (JM), (f)
 195 Pt/CNTs, and (g) Pt/CCNTs.

196 As a comparison, the TEM images of XC-72 and CNTs are shown in Fig. 5a and Fig.
 197 5b. XC-72 consists of spherical carbon particles with diameters of 20~50 nm. Fig. 5c
 198 displays crystalline structure of CCNTs particles consisting of the graphitic coils with
 199 a wall thickness of 5-10 nm. The observed graphitic layers are consistent with the
 200 above XRD results. Fig. 5e and Fig. 5f clearly reveal Pt particles distributed
 201 uniformly with a size ranging from 3 to 4 nm on XC-72 and a size distribution of 5-7
 202 nm on CNTs. As shown in Fig. 5g, Pt particles with size ranging from 3 to 5 nm are
 203 homogeneously dispersed over the CCNTs, which agrees well with the calculated
 204 results from XRD.

205 *3.2. Electrochemical measurements of the electrocatalysts*



206



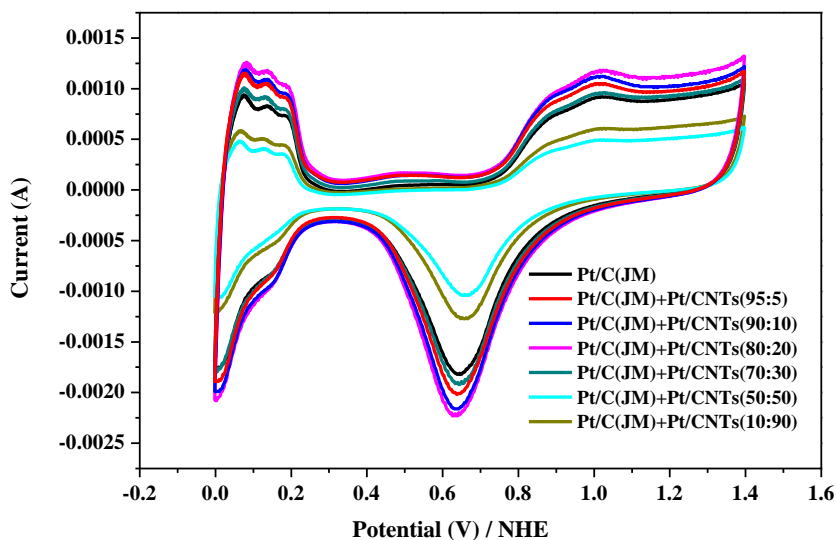
207

208 **Fig. 6.** Cyclic voltammograms of (a) Pt/CCNTs and CCNTs, and (b) Pt/C (JM),
 209 Pt/CCNTs, and Pt/CNTs catalysts in 0.5 M H₂SO₄ with a scan rate of 20 mV s⁻¹ at
 210 room temperature.

211 The cyclic voltammograms of Pt/CCNTs and CCNTs are shown in Fig. 6a. The
 212 ECSA of Pt can be calculated using Eq. (1) from the hydrogen electrooxidation peak
 213 after subtraction of the double layer capacitance [26]. The charge of full coverage for
 214 clean polycrystalline Pt is $Q_H = 210 \mu\text{C cm}^{-2}$. L_{Pt} is the Pt loading on the working
 215 electrode and A_g is the geometric surface area of the glassy carbon electrode.

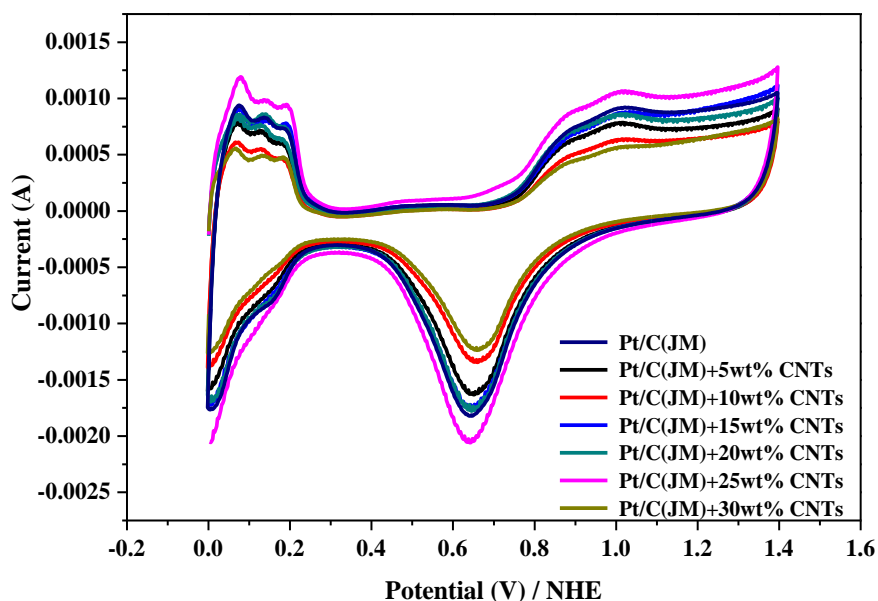
$$216 \text{ ECSA (m}^2 \text{ g}_{\text{Pt}}^{-1}) = \left[\frac{Q_H \text{ (C)}}{210 \mu\text{C cm}_{\text{Pt}}^{-2} L_{\text{Pt}} \text{ (mg}_{\text{Pt}} \text{ cm}^{-2}) A_g \text{ (cm}^2)} \right] 10^5 \quad (1)$$

217 Fig. 6b shows cyclic voltammograms of Pt-electrocatalysts scanned from 0 to 1.4 V
 218 vs. NHE at a scan rate of 20 mV s⁻¹ in 0.5 M H₂SO₄. According to Eq. (1), the ECSAs
 219 for Pt/C (JM), Pt/CNTs, and Pt/CCNTs are calculated to be 70, 38, and 65 m² g_{Pt}⁻¹,
 220 respectively. The result is consistent with the mean size of Pt obtained from XRD
 221 corresponding to 3.5 nm, 5.8 nm, and 3.7 nm, respectively. Although the activities for
 222 Pt/CNTs and Pt/CCNTs are inferior compared to commercial Pt/C, additions of
 223 Pt/CNTs and/or Pt/CCNTs into the Pt/C (JM) catalyst can improve the catalytic
 224 activity of the commercial catalyst significantly, as shown by the results given below.



225

226 **Fig. 7.** Cyclic voltammograms of the mixed Pt/C and Pt/CNTs catalysts in 0.5 M
 227 H₂SO₄ at 25 °C at a scan rate of 20 mV s⁻¹.



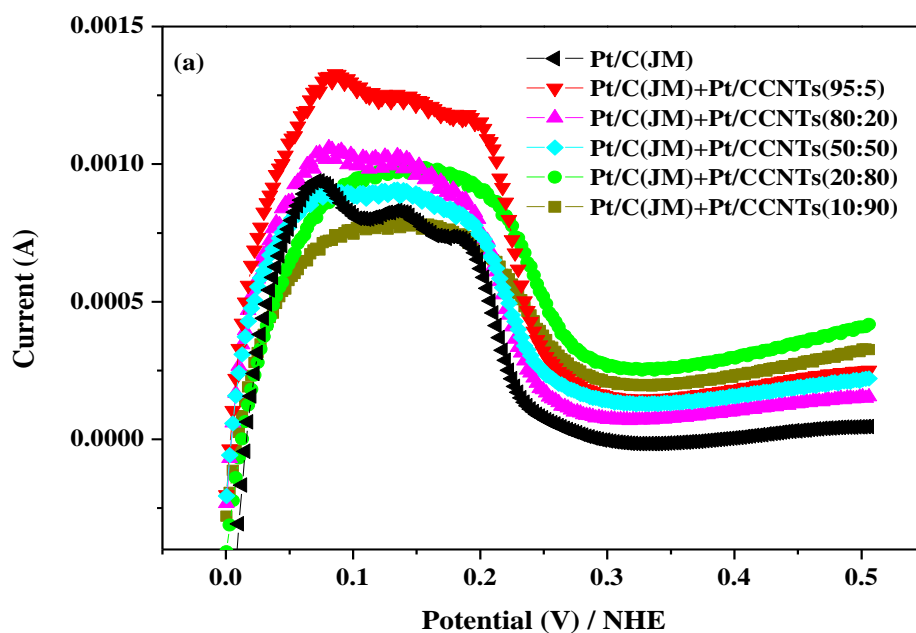
228

229 **Fig. 8.** Cyclic voltammograms of Pt/C with addition of different amounts of CNTs in
 230 0.5 M H₂SO₄ at 25 °C at a scan rate of 20 mV s⁻¹.

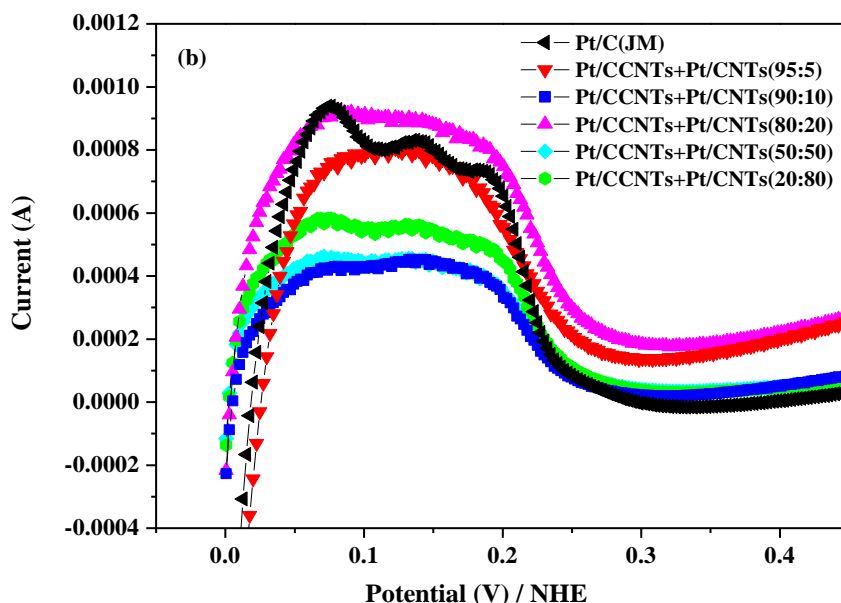
231 Firstly, ECSAs for mixed catalysts of each two kinds of Pt catalysts with different
 232 mass ratios are evaluated from CV. CV curves of the mixed Pt/C and Pt/CNTs
 233 catalysts with mass ratios of 70:30, 80:20, 90:10, and 95:5 are shown in Fig. 7, and
 234 their corresponding ECSA are 74, 90, 84, and 79 m² g_{Pt}⁻¹, respectively. The optimum
 235 ratio of Pt/C to Pt/CNTs is 80:20, its ECSA is 20 m² g_{Pt}⁻¹ higher than that of Pt/C (JM)

236 catalyst, even the individual Pt/CNTs show much lower activity. It is most likely due
237 to the fact that CNTs form a multi-dimensional network structure and establish a
238 better conductive path [27]. However, if more than 50 wt% of Pt/CNTs is added, a
239 decrease in ECSA is observed. This is mainly due to the less catalytic activity
240 contribution originating from Pt/CNTs.

241 In order to explore the role of CNTs, CVs of Pt/C with different amounts of CNTs
242 were recorded as shown in Fig. 8. It can be seen that Pt/C with 25wt% CNTs exhibits
243 the highest ECSA of $135.5 \text{ m}^2 \text{ g}_{\text{Pt}}^{-1}$, which is obviously higher than that of Pt/C with
244 5wt% CNTs, 10wt% CNTs, 15wt% CNTs, 20wt% CNTs, and 30wt% CNTs, and their
245 corresponding ECSAs are 77, 78, 88, 100, and $79 \text{ m}^2 \text{ g}_{\text{Pt}}^{-1}$, respectively. The results
246 indicate that adding too large or too small amounts of CNTs induces a decrease in
247 ECSA. With the CNTs content increasing, the ECSA increases at first which can be
248 attributed to the formation of a porous network structure, but decreases with the
249 excess amount of CNTs because CNTs itself does not have catalytic activity.



250

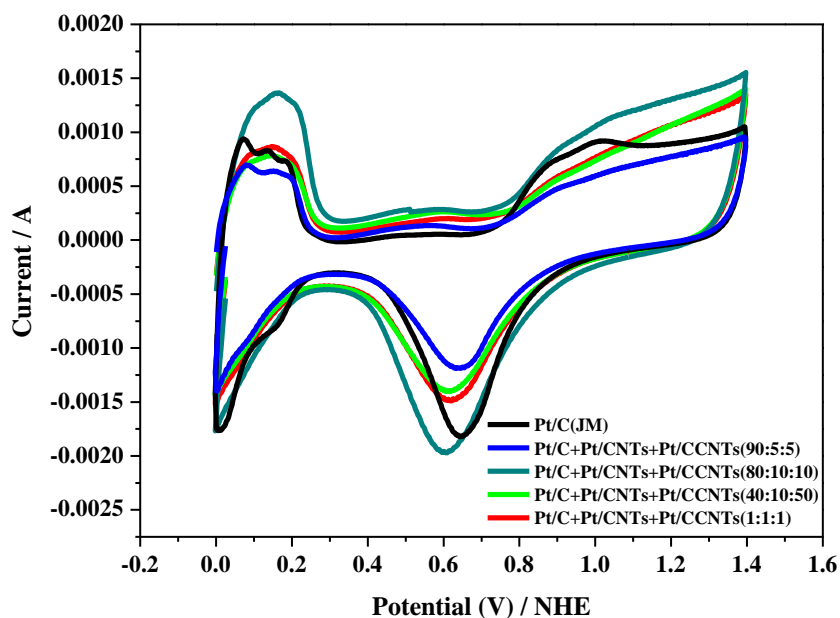


251

252 **Fig. 9.** Cyclic voltammograms of (a) the mixed Pt/C with Pt/CCNTs, and (b) mixed
 253 Pt/CCNTs with Pt/CNTs in 0.5M H₂SO₄ at 25 °C at a scan rate of 20 mV s⁻¹ [Only
 254 part CV curves were shown in a potential window of -0.0 to +0.5 V].

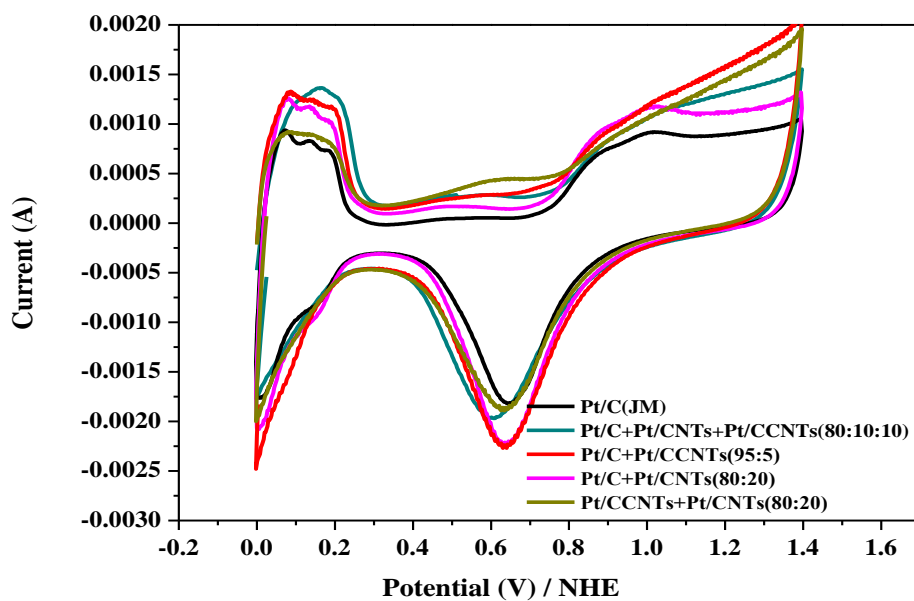
255 ECSA data calculated from Fig. 9a show that the optimum ratio of Pt/C to Pt/CCNTs
 256 is 95:5 with the ECSA value of 106 m² g_{Pt}⁻¹. According to the BJH results, CCNTs
 257 exhibit a uniform pore size distribution (10-40 nm) and better pore volume with the
 258 increased special surface area. It proves that a very small amount of three-dimensional
 259 porous CCNTs incorporated with zero-dimensional XC-72 could contribute to a

260 higher ECSA. Meanwhile, the mixed Pt/CCNTs and Pt/CNTs catalysts with mass
 261 ratio of 80:20 as shown in Fig. 9b shows a similar ECSA value of $69 \text{ m}^2 \text{ g}_{\text{Pt}}^{-1}$ to that of
 262 Pt/C (JM) catalyst, even individual Pt/CCNTs or Pt/CNTs catalyst demonstrate poor
 263 catalytic activity.



264

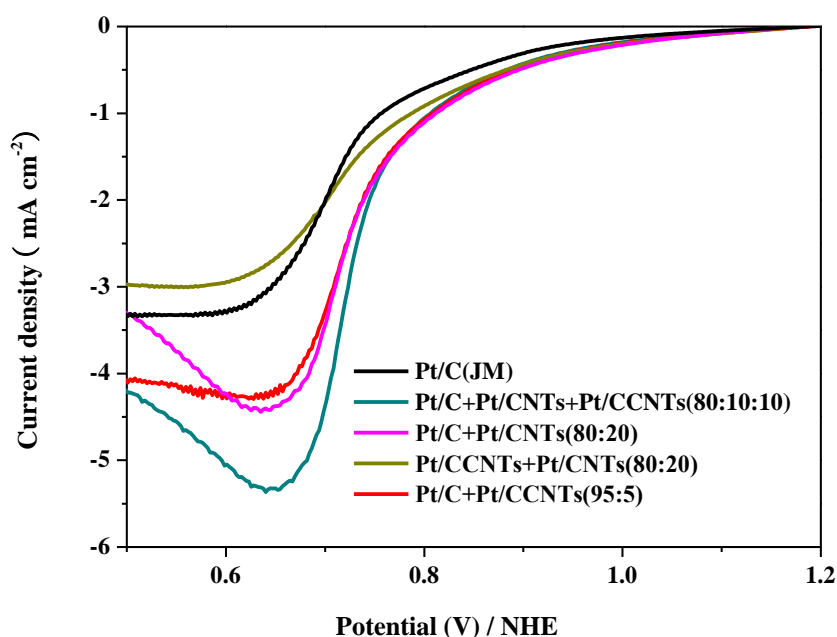
265 **Fig. 10.** Cyclic voltammograms of the mixed Pt/C with Pt/CNTs and Pt/CCNTs in 0.5
 266 M H_2SO_4 at 25°C at a scan rate of 20 mV s^{-1} .



267

268 **Fig. 11.** Cyclic voltammograms of the optimum electrocatalysts in 0.5 M H₂SO₄ at 25
269 °C at a scan rate of 20 mV s⁻¹.

270 In Fig. 10, the mixed Pt/C, Pt/CNTs, and Pt/CCNTs with mass ratios of 80:10:10
271 produce the highest ECSA value of 111 m² g_{Pt}⁻¹. The three kinds of the above
272 mentioned catalysts with mass ratio of 40:10:50 or 1:1:1 exhibit a similar integrated
273 charge with Pt/C (JM) in the hydrogen absorption region. However, more than 80wt%
274 of Pt/C leads to an ECSA decrease, because it needs more CNTs or CCNTs to
275 construct a multi-dimensional structure and to contact well with each other [28]. CVs
276 of the optimized two and three kinds of mixed catalysts are shown in Fig. 11. The
277 remarkable enhanced activity of Pt/C-Pt/CNTs-Pt/CCNTs can be explained in three
278 aspects. Firstly, the multilayer compressed structure is avoided due to the addition of
279 one-dimensional Pt/CNTs and three-dimensional Pt/CCNTs. Additionally, Pt/CCNTs-
280 Pt/CNTs work as a multi-dimensional network, promoting electrolyte through the
281 surface of catalysts. Ultimately, we can suggest that the catalytic activity contribution
282 mainly originated from Pt/C. However, the mixed Pt/C with appropriate amounts of
283 Pt/CNTs and/or Pt/CCNTs offered much higher ECSA values.



284

285 **Fig. 12.** Polarization curves of the optimum electrocatalysts in O₂-saturated 0.5 M
286 H₂SO₄ at 25 °C at a scan rate of 10 mV s⁻¹ and rotation rate of 1600 rpm.

287 RDE measurements are taken to evaluate the ORR activity of catalysts. Fig. 12 shows
288 polarization curves with RDE for the mixed two and three kinds of catalysts. The
289 onset potential of the mixed Pt/C-Pt/CNTs-Pt/CCNTs catalysts with mass ratio of
290 80:10:10 is 0.91 V and similar to the commercial Pt/Ccatalyst. At potential of 0.7 V,

291 the current densities of the Pt/C-Pt/CNTs-Pt/CCNTs, Pt/C-Pt/CCNTs, Pt/C-Pt/CNTs,
292 and Pt/CCNTs-Pt/CNTs are 4.7, 3.4, 3.2, and 2.2 mA cm⁻², compared to 2.1 mA cm⁻²
293 of Pt/C, indicate that the mixture of two or three kinds of catalysts exhibit better ORR
294 activity. This improvement can be attributed to the more efficient mass transport in
295 the higher current density regions, facilitating O₂ diffusion among the catalyst layer
296 and promoting access to Pt active sites. These results are consistent with the increased
297 ECSAs obtained from CVs.

298 The electrocatalytic reaction region involves solid, liquid, and gas phase mass
299 transport and electron/proton transfer [25]. Based on the morphology of the three-
300 phase region, two and three kinds of mixed electrocatalysts are employed to construct
301 a multi-dimensional network for the sake of optimizing the electrode structure:
302 allowing the reactant more easily to get access to the active sites and the product to be
303 quickly removed from them, facilitating electron/proton transfer, thus assuring that
304 the reaction goes smoothly. The unique structure of Pt/C-Pt/CNTs-Pt/CCNTs is
305 advantageous for the ORR pathway compared to the individual Pt/CNTs, Pt/CCNTs
306 or Pt/C. XC-72 is a good support to disperse precious metal particles, CNTs play the
307 role of transferring electrons, and CCNTs are responsible for constructing preferable
308 mass transport channels. Finally, we conceive that the mixed Pt/C with Pt/CNTs and
309 Pt/CCNTs could be used to offer more active sites, more favorable gas-diffusion
310 channels, and lower resistant charge-transfer paths.

311 **4. Conclusions**

312 In this research, each two and three kinds of Pt/C, Pt/CNTs, and Pt/CCNTs are mixed
313 with different mass ratios. The specific active surface areas of the mixed Pt/C and
314 Pt/CCNTs with mass ratio of 95:5 and mixed Pt/C with Pt/CNTs and Pt/CCNTs with
315 mass ratio of 80:10:10 are calculated to be 106 m² g_{Pt}⁻¹ and 111 m² g_{Pt}⁻¹ with respect to
316 70 m² g_{Pt}⁻¹ for commercial Pt/C catalyst due to the unique structure of CCNTs and the
317 enhanced conductivity of CNTs. RDE results also confirm the improved ORR activity
318 of the mixed Pt/C with Pt/CNTs and/or Pt/CCNTs. These results indicate that two and
319 three of the mixed platinum electrocatalysts supported on various carbon materials
320 can significantly enhance the performance and utilization of the catalysts, and this
321 result can be applied for practical fuel cell stacks to better the performance and reduce
322 the amount of catalyst.

323

324 **Acknowledgements**

325 This work was supported by the Technology Project of Education Department of
326 Sichuan Province (13ZA0193), Innovative Research Team of Southwest Petroleum
327 University (2012XJZT002), and Scientific Research Foundation for Returned
328 Scholars, Ministry of Education of China.

329

330 **References**

- 331 [1] E. Reddington, A. Sapienza, B. Gurau, R. Viswanathan, S. Sarangapani, E.S.
332 Smotkin, T.E. Mallouk, *Science* 280 (1998) 1735-1737.
- 333 [2] M. Hogarth, T. Ralph, *Platinum Met. Rev.* 46 (2002) 146-164.
- 334 [3] T.S. Ahmadi, Z.L. Wang, T.C. Green, A. Henglein, M.A. El-Sayed, *Science* 272
335 (1996) 1924-1925.
- 336 [4] M.K. Debe, *Nature* 486 (2012) 43-51.
- 337 [5] S.H. Tang, G.Q. Sun, J. Qi, S.G. Sun, J.S. Guo, Q. Xin, G.M. Haarberg, *Chin. J.*
338 *Catal.* 31 (2010) 12-17.
- 339 [6] J.S. King, A. Wittstock, J. Biener, S.O. Kucheyev, Y.M. Wang, T.F. Baumann,
340 S.K. Giri, A.V. Hamza, M. Baeumer, S.F. Bent, *Nano Lett.* 8 (2008) 2405-2409.
- 341 [7] R.Z. Yang, X.P. Qiu, H.R. Zhang, J.Q. Li, W.T. Zhu, Z.X. Wang, X.J. Huang,
342 L.Q. Chen, *Carbon* 43 (2005) 11-16.
- 343 [8] N. Punbusayakul, S. Talapatra, L. Ci, W. Surareungchai, P.M. Ajayan,
344 *Electrochem. Solid-State. Lett.* 10 (2007) 13-17.
- 345 [9] C. Soldano, S. Kar, S. Talapatra, S. Nayak, P.M. Ajayan, *Nano Lett.* 8 (2008)
346 4498-4505.
- 347 [10] S. Talapatra, S. Kar, S.K. Pal, R. Vajtai, L. Ci, P. Victor, M. Shaijumon, S. Kaur,
348 O. Nalamasu, P.M. Ajayan, *Nat. Nano* 1 (2006) 112-116.
- 349 [11] T. Hyeon, S. Han, Y. E. Sung, K. W. Park, Y. W. Kim, *Angew. Chem. Int. Ed.*
350 42 (2003) 4488-4492.
- 351 [12] P. Ramesh, M.E. Itkis, J.M. Tang, R.C. Haddon, *J. Phys. Chem. C* 112 (2008)
352 9089-9094.
- 353 [13] M.M. Shaijumon, S. Ramaprabhu, N. Rajalakshmi, *Appl. Phys. Lett.* 88 (2006)
354 253105-253105-3.
- 355 [14] S. Stankovich, D.A. Dikin, G.H.B. Dommett, K.M. Kohlhaas, E.J. Zimney, E.A.
356 Stach, R.D. Piner, S.T. Nguyen, R.S. Ruoff, *Nature* 442 (2006) 282-286.
- 357 [15] N. Behabtu, J.R. Lomeda, M.J. Green, A.L. Higginbotham, A. Sinitskii, D.V.
358 Kosynkin, D. Tsentelovich, A.N.G. Parra-Vasquez, J. Schmidt, E. Kesselman, Y.
359 Cohen, Y. Talmon, J.M. Tour, M. Pasquali, *Nat. Nano* 5 (2010) 406-411.
- 360 [16] S.D. Yang, C.M. Shen, X.J. Lu, H. Tong, J.J. Zhu, X.G. Zhang, H.J. Gao,
361 *Electrochim. Acta* 62 (2012) 242-249.

362 [17] R. I. Jafri, T. Arockiados, N. Rajalakshmi, S. Ramaprabhu, *J. Electrochem. Soc.*
363 157 (2010) 874-879.

364 [18] J. Qi, L.H. Jiang, S.L. Wang, G.Q. Sun, *Appl. Catal. B* 107 (2011) 95-103.

365 [19] G.S. Chai, I.S. Shin, J. S. Yu, *Adv. Mater.* 16 (2004) 2057-2061.

366 [20] N.P. Subramanian, S.P. Kumaraguru, H. Colon-Mercado, H. S. Kim, B.N.
367 Popov, T. Black, D.A. Chen, *J. Power Sources* 157 (2006) 56-63.

368 [21] M. Sevilla, C. Sanchís, T. Valdés-Solís, E. Morallón, A.B. Fuertes, *J. Phys.*
369 *Chem. C* 111 (2007) 9749-9756.

370 [22] K. W. Park, Y. E. Sung, S. Han, Y. Yun, T. Hyeon, *J. Phys. Chem. B* 108 (2004)
371 939-944.

372 [23] M.A. Pimenta, G. Dresselhaus, M.S. Dresselhaus, L.A. Cancodo, A. Jorio, R.
373 Sato, *Phys. Chem. Chem. Phys.* 9 (2007) 1276-1290.

374 [24] S. Mukerjee, S. Srinivasan, M.P. Soriaga, J. McRreen, *J. Electrochem. Soc.* 142
375 (1995) 1409-1422.

376 [25] S. Litster, G. Mclean, *J. Power Sources* 130 (2004) 61-76.

377 [26] Y. Garsany, O.A. Baturina, K.E. Swider-Lyons, S.S. Kocha, *Anal. Chem.* 82
378 (2010) 6321-6328.

379 [27] P. Wu, B. Li, H.D. Du, L. Gan, F.Y. Kang, Y.Q. Zeng, *J. Power Sources* 184
380 (2008) 381-384.

381 [28] C. F. Chi, M. C. Yang, H. S Weng, *J. Power Sources* 193 (2009) 462-469.

382